 FDMP, vol.4, no.3, pp.185-197, 2008

Nonlinear Development of Interfacial Instability in a Thin Two-Layer Liquid Film in the Presence of Van-Der-Waals Interactions

A. A. Nepomnyashchy[1,2] **and I. B. Simanovskii**[1]

Abstract: The development of instabilities under the joint action of the van der Waals forces and Marangoni stresses in a two-layer film on a heated or cooled substrate is considered. It is found that heating from below leads to the acceleration of the decomposition, decrease of the characteristic lateral size of structures, and the increase of the droplets heights. Heating from above leads to slowing down the instability rate and eventually to a complete suppression of the instability.

1 Introduction

Two-layer fluid systems are widespread in numerous branches of technology, including chemical engineering, space technologies, coating, etc. When the thicknesses of layers are sufficiently thin, the flows are strongly affected by interfacial phenomena, specifically by the Marangoni effect (13), (8).

In the past few decades, the development of microfluidics and nanotechnology led to a significant progress in exploration of thin film flows. Such kind of flows has numerous technological applications (coating, flotation, biological membranes, adhesives etc.). The instabilities in thin films are of potential use in the formation of regular nanostructures and ordered porous membranes, in soft-lithographic techniques and in other areas of nanotechnology.

The dynamics of ultra-thin (but still macroscopic) films, with the thickness less than 100 nm, is of a special interest. In the case of ultra-thin films, it is necessary to take into account the long-range intermolecular forces (first of all, van der Waals forces) acting between molecules of the liquid and substrate (4). A theoretical description of two-layer ultra-thin films has been developed in Refs. (10)-(12).

The dynamics of ultra-thin films under the joint action of the Marangoni effect and the van der Waals forces has not yet been extensively explored. In (6), (11), a general structure of the evolution equation has been considered. The case of a temperature gradient directed along the interfaces has been studied in (7).

In the present paper, we consider the development of instabilities under the joint action of the van der Waals forces and Marangoni stresses in a two-layer film on a heated or cooled substrate. The mathematical model is developed in Sec. 2. Sec. 3 is devoted to numerical simulations of the nonlinear problem. A summary of results is given in Sec. 4.

2 Long-wave evolution equations

2.1 Thermocapillary flow

2.1.1 Formulation of the problem

Consider a system of two superposed layers of immiscible liquids with different physical properties (see Fig. 1). The bottom layer rests on a solid substrate, the top layer is in contact with the adjacent gas phase. The temperature of the solid substrate is T_s, the temperature of the gas is T_g. All the variables referring to the bottom layer are marked by subscript 1, and all the variables referring to the top layer are marked by subscript 2. The equilibrium thicknesses of the layers are H_i^0, $i = 1,2$. The deformable interfaces are described by equations $z = H_1(x,y,t)$ (liquid-liquid interface) and $z = H_2(x,y,t)$ (liquid-gas in-

[1] Department of Mathematics, Technion – Israel Institute of Technology, 32000, Haifa, Israel

[2] Minerva Center for Nonlinear Physics of Complex Systems, Technion – Israel Institute of Technology, 32000, Haifa, Israel

terface). The ith fluid has density ρ_i, kinematic viscosity ν_i, dynamic viscosity $\eta_i = \rho_i \nu_i$, thermal diffusivity χ_i and heat conductivity κ_i. The surface tension coefficients on the lower and upper interfaces, σ_1 and σ_2, are linear functions of temperature T: $\sigma_1 = \sigma_1^0 - \alpha_1 T$, $\sigma_2 = \sigma_2^0 - \alpha_2 T$. The effect of gravity is neglected. The intermolecular forces are neglected in the present subsection.

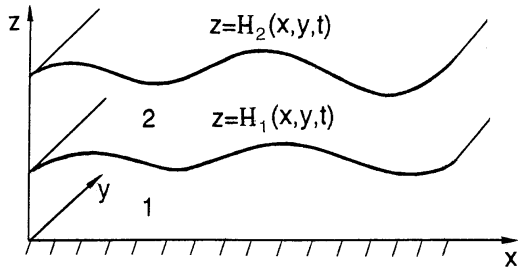

Figure 1: Geometric configuration of the region and coordinate axes.

The complete system of nonlinear equations governing Marangoni convection are written in the following form (13):

$$\frac{\partial \mathbf{v}_i}{\partial t} + (\mathbf{v}_i \nabla)\mathbf{v}_i = -\frac{1}{\rho_i}\nabla P_i + \nu_i \Delta \mathbf{v}_i, \tag{1}$$

$$\frac{\partial T_i}{\partial t} + \mathbf{v}_i \nabla T_i = \frac{1}{\chi_i}\Delta T_i, \tag{2}$$

$$\nabla \cdot \mathbf{v}_i = 0,\ i = 1,2. \tag{3}$$

The boundary conditions on the rigid boundary are:

$$\mathbf{v}_1 = 0, T_1 = T_s;\ \text{at}\ \ z = 0. \tag{4}$$

On the deformable interface $z = H_1$, the following boundary conditions hold: the balance of normal stresses,

$$P_2 - P_1 + 2\sigma_1 K_1 = \left[-\eta_1\left(\frac{\partial v_{1i}}{\partial x_k} + \frac{\partial v_{1k}}{\partial x_i}\right) + \eta_2\left(\frac{\partial v_{2i}}{\partial x_k} + \frac{\partial v_{2k}}{\partial x_i}\right)\right] \cdot n_{1i} n_{1k}; \tag{5}$$

the balance of tangential stresses,

$$\left[-\eta_1\left(\frac{\partial v_{1i}}{\partial x_k} + \frac{\partial v_{1k}}{\partial x_i}\right) + \eta_2\left(\frac{\partial v_{2i}}{\partial x_k} + \frac{\partial v_{2k}}{\partial x_i}\right)\right] \cdot \tau_{1i}^{(l)} n_{1k} - \alpha_1 \tau_{1i}^{(l)} \frac{\partial T_1}{\partial x_i} = 0, \quad l = 1,2; \tag{6}$$

the continuity of the velocity field,

$$\mathbf{v}_1 = \mathbf{v}_2; \tag{7}$$

the kinematic equation for the interface motion,

$$\frac{\partial H_1}{\partial t} + v_{1x}\frac{\partial H_1}{\partial x} + v_{1y}\frac{\partial H_1}{\partial y} = v_{1z}; \tag{8}$$

the continuity of the temperature field,

$$T_1 = T_2; \tag{9}$$

and the balance of normal heat fluxes,

$$\left(\kappa_1 \frac{\partial T_1}{\partial x_i} - \kappa_2 \frac{\partial T_2}{\partial x_i}\right) n_{1i} = 0. \tag{10}$$

Similar boundary conditions are imposed on the deformable interface $z = H_2$:

$$-P_2 + 2\sigma_2 K_2 = -\eta_2\left(\frac{\partial v_{2i}}{\partial x_k} + \frac{\partial v_{2k}}{\partial x_i}\right) n_{2i} n_{2k}, \tag{11}$$

$$-\eta_2\left(\frac{\partial v_{2i}}{\partial x_k} + \frac{\partial v_{2k}}{\partial x_i}\right)\tau_{2i}^{(l)} n_{2k} - \alpha_2 \tau_{2i}^{(l)} \frac{\partial T_3}{\partial x_i} = 0, \quad l = 1,2, \tag{12}$$

$$\frac{\partial H_2}{\partial t} + v_{2x}\frac{\partial H_2}{\partial x} + v_{2y}\frac{\partial H_2}{\partial y} = v_{2z}, \tag{13}$$

K_1 and K_2 are the mean curvatures, $\mathbf{n_1}$ and $\mathbf{n_2}$ are the normal vectors and $\tau_1^{(l)}$ and $\tau_2^{(l)}$ are the tangential vectors of the lower and upper interfaces; P_i is the difference between the overall pressure and the atmospheric pressure. For a heat flux on the liquid-gas interface we use an empirical condition,

$$\kappa_2 \frac{\partial T_2}{\partial x_i} n_{2i} = -q(T - T_g), \tag{14}$$

where q is the heat exchange coefficient which is assumed to be constant.

2.1.2 Derivation of the longwave amplitude equation

The system of equations and boundary conditions (1)-(14) is rather complicated. However, in the case of thin film flows, when the fluid system is

thin in one direction and extended in other directions, the nonlinear model governing three-dimensional flows with a deformable interface can be drastically simplified by means of a *long-wavelength expansion*. The leading order of this expansion is known as *the lubrication approximation*. The longwave approach is based on the assumption that the characteristic spatial scales in the directions x and y are much larger than that in the direction z. It is assumed that the solution of equations and boundary conditions (1)-(14) depends on the scaled horizontal coordinates $X = \varepsilon x$ and $Y = \varepsilon y$, $\varepsilon \ll 1$, rather than on x and y. Also, it is assumed that the solution depends on the scaled time variable $\tau = \varepsilon t$. The details of the longwave approach applied to thermocapillary flows can be found in review papers (2), (9).

At the leading order, the evolution of the system is governed by the following equations and boundary conditions:

$$\begin{aligned} &U_{1zz} = 0;\ V_{1zz} = 0;\ U_{1X} + V_{1Y} + W_{1z} = 0; \\ &T_{1zz} = 0;\ 0 < z < H_1; \end{aligned} \tag{15}$$

$$\begin{aligned} &U_{2zz} = 0;\ V_{2zz} = 0;\ U_{2X} + V_{2Y} + W_{2z} = 0; \\ &T_{2zz} = 0;\ H_1 < z < H_2; \end{aligned} \tag{16}$$

$$z = 0:\ U_1 = V_1 = W_1 = 0;\ T_1 = T_s; \tag{17}$$

$$z = H_1:\ U_1 = U_2;\ V_1 = V_2;\ W_1 = W_2; \tag{18}$$

$$\eta_2 U_{2z} - \eta_1 U_{1z} - \alpha_1 (T_{1X} + H_{1X} T_{1z}) = 0; \tag{19}$$

$$\eta_2 V_{2z} - \eta_1 V_{1z} - \alpha_1 (T_{1Y} + H_{1Y} T_{1z}) = 0; \tag{20}$$

$$H_{1\tau} + U_1 H_{1X} + V_1 H_{1Y} = W_1; \tag{21}$$

$$T_1 = T_2;\ \kappa_1 T_{1z} = \kappa_2 T_{2z}; \tag{22}$$

$$z = H_2:\ -\eta_2 U_{2z} - \alpha_2 (T_{2X} + H_{2X} T_2) = 0; \tag{23}$$

$$-\eta_2 V_{2z} - \alpha_2 (T_{2Y} + H_{2Y} T_{2z}) = 0; \tag{24}$$

$$H_{2\tau} + U_2 H_{2X} + V_2 H_{2Y} = W_2; \tag{25}$$

$$\kappa_2 T_{2z} = -q(T - T_g), \tag{26}$$

where subscripts z, X, Y and τ denote corresponding partial derivatives, U_j, V_j and W_j, $j = 1, 2$ are the leading-order terms in the expansions in powers of ε:

$$u_{xj} = U_j + \ldots,\ u_{yj} = V_j + \ldots,\ u_{zj} = \varepsilon W_j + \ldots.$$

Solving the problem for the temperature fields, we find:

$$T_1 = T_s - (T_s - T_g) D q \kappa_2 z; \tag{27}$$

$$T_2 = T_s - (T_s - T_g) D q [(\kappa_2 - \kappa_1) H_1 + \kappa_1 z], \tag{28}$$

where

$$D = [\kappa_1 \kappa_2 + q(\kappa_2 - \kappa_1) H_1 + q \kappa_1 H_2]^{-1}. \tag{29}$$

The x-components of the flow generated by the thermocapillary stresses is determined by the following formulas:

$$U_1 = \frac{(T_s - T_g)\kappa_2}{\eta_1} [D(\alpha_1 q H_1 - \alpha_2 \kappa_1)]_X z, \tag{30}$$

$$\begin{aligned} U_2 = \frac{(T_s - T_g)\kappa_2}{\eta_2} \{ &-\alpha_2 \kappa_2 D_X z \\ &+ \frac{H}{\eta_1} [D(\alpha_1 \eta_2 q H_1 - \alpha_2 (\eta_2 - \eta_1)\kappa_1)_X]_X \Big\}. \end{aligned} \tag{31}$$

The expressions for y-components of the flow, V_1 and V_2, can be obtained from U_1 and U_2 by replacing X by Y. Solving the continuity equations with respect to W_1 and W_2 with corresponding boundary conditions, we find that

$$W_1(X, Y, H_1) = -\int_0^{H_1} (U_{1X} + V_{1Y}) dz, \tag{32}$$

$$\begin{aligned} W_2(X, Y, H_2) = &-\int_0^{H_1} (U_{1X} + V_{1Y}) dz \\ &+ \int_{H_1}^{H_2} (U_{2X} + V_{2Y}) dz. \end{aligned} \tag{33}$$

Using (32) and (33), we rewrite the kinematic conditions (21) and (25) in the following form:

$$H_{1\tau} + \left(\int_0^{H_1} U_1 dz \right)_X + \left(\int_0^{H_1} V_1 dz \right)_Y = 0; \tag{34}$$

$$\begin{aligned} H_{2\tau} + &\left(\int_0^{H_1} U_1 dz + \int_{H_1}^{H_2} U_2 dz \right)_X \\ &+ \left(\int_0^{H_1} V_1 dz + \int_{H_1}^{H_2} V_2 \right)_Y = 0. \end{aligned} \tag{35}$$

Substituting expressions for flow velocities obtained above into equations (34), (35), we arrive to a closed system of equations that govern the evolution of a heated two-layer film under the action of the thermocapillary effect:

$$H_{1\tau}+\nabla\cdot\mathbf{Q}_1^T=0,\ H_{2\tau}+\nabla\cdot\mathbf{Q}_2^T=0, \tag{36}$$

where

$$\mathbf{Q}_1^T=\frac{(T_s-T_g)\kappa_2}{2\eta_1}H_1^2\nabla[D(q\alpha_1H_1-\alpha_1\kappa_1)], \tag{37}$$

$$\mathbf{Q}_2^T=\frac{(T_s-T_g)}{2\eta_1\eta_2}\Big\{H_2^2\nabla[(-\alpha_2\kappa_1\eta_1)D]+(2H_2-H_1)\cdot H_1\nabla\big\{D[q\alpha_1\eta_2H_1-\alpha_2\kappa_1(\eta_2-\eta_1)]\big\}\Big\}. \tag{38}$$

2.2 Flows in the presence of van der Waals forces

In the framework of the continuum approach, the van der Waals forces manifest themselves as an external normal stresses ("disjoining pressures") imposed on each interface (4)-(12). The disjoining pressures modify the dependencies of the pressures P_1 and P_2 in each layer on the layers thicknesses H_1 and H_2 in the following way (3):

$$P_1=-\sigma_1\nabla^2H_1-\sigma_2\nabla^2H_2+W_1(H_1,H_2), \tag{39}$$

$$P_2=-\sigma_2\nabla^2H_2+W_2(H_1,H_2), \tag{40}$$

where

$$W_1(H_1,H_2)=\frac{A_{sg}-A_{s2}-A_{g1}}{6\pi H_2^3}+\frac{A_{s2}}{6\pi H_1^3}, \tag{41}$$

$$W_2(H_1,H_2)=\frac{A_{sg}-A_{s2}-A_{g1}}{6\pi H_2^3}+\frac{A_{g1}}{6\pi(H_2-H_1)^3}. \tag{42}$$

Here A_{sg}, A_{s2} and A_{g1} are Hamaker constants characterizing the interactions between the solid substrate and the gas across the two layers, between the solid substrate and liquid 2 across liquid 1, and between the gas phase and liquid 1 across liquid 2, correspondingly.

It was shown earlier (11), (7) that in the framework of the lubrication approximation the influence of the surface tension and van der Waals forces on the dynamics of a non-isothermic two-layer thin film is described by additional flux terms in evolution equations:

$$\begin{aligned}&H_{1\tau}+\nabla\cdot(\mathbf{Q}_1^T+\mathbf{Q}_1^{vdW})=0,\\&H_{2\tau}+\nabla\cdot(\mathbf{Q}_2^T+\mathbf{Q}_2^{vdW})=0,\end{aligned} \tag{43}$$

where

$$\begin{aligned}&\mathbf{Q}_1^{vdW}=\mathbf{Q}_1^0=F_{11}\nabla P_1+F_{12}\nabla P_2,\\&\mathbf{Q}_2^{vdW}=F_{21}\nabla P_1+F_{22}\nabla P_2.\end{aligned} \tag{44}$$

The pressures P_1 and P_2 are determined by expressions (39), (40), and the mobility functions are:

$$F_{11}=-\frac{1}{3\eta_1}H_1^3;\quad F_{12}=-\frac{1}{2\eta_1}H_1^2(H_2-H_1);$$

$$F_{21}=\frac{1}{6\eta_1}H_1^3-\frac{1}{2\eta_1}H_1^2H_2;$$

$$F_{22}=(H_2-H_1)\left[H_1^2\left(\frac{1}{2\eta_1}-\frac{1}{3\eta_2}\right)+H_1H_2\left(-\frac{1}{\eta_1}+\frac{2}{3\eta_2}\right)-\frac{1}{3\eta_2}H_2^2\right].$$

Following (3), we choose the initial thickness of the lower layer, H_1^0, as the vertical length scale, and the quantities $\lambda^*=(H_1^0)^2\sqrt{6\pi\sigma_1^0/|A_{sg}|}$, $\tau^*=36\pi^2\sigma_1^0\eta_1(H_1^0)^5/A_{sg}^2$, and $p^*=|A_{sg}|/6\pi(H_1^0)^3$ as the horizontal length scale, time scale, and pressure scale, respectively. Equations (43) are written in the dimensionless form,

$$h_{1\tau}+\nabla\cdot\mathbf{q}_1=0,\quad h_{2\tau}+\nabla\cdot\mathbf{q}_2=0, \tag{45}$$

$$\begin{aligned}&\mathbf{q}_1=f_{11}\nabla p_1+f_{12}\nabla p_2+\mathbf{q}_1^T,\\&\mathbf{q}_2=f_{21}\nabla p_1+f_{22}\nabla p_2+\mathbf{q}_2^T;\end{aligned} \tag{46}$$

where $T=t/\tau^*$, $h_j=H_j/H_1^0$, $p_j=P_j/p^*$, $j=1,2$,

$$f_{11}=-\frac{1}{3}h_1^3,\quad f_{12}=-\frac{1}{2}h_1^2(h_2-h_1),$$

$$f_{21}=\frac{1}{6}h_1^3-\frac{1}{2}h_1^2h_2,$$

$$f_{22}=(h_2-h_1)\left[h_1^2\left(\frac{1}{2}-\frac{\eta}{3}\right)+h_1h_2\left(-1+\frac{2\eta}{3}\right)-\frac{\eta}{3}h_2^2\right].$$

Later on, we assume that the dependence of interfacial tensions on the temperature is relatively weak and can be neglected in the boundary conditions for *normal stresses* (but not in those for tangential stresses where it is the source of a thermocapillary motion). The pressures include the disjoining potentials:

$$p_1 = -\nabla^2 h_1 - \sigma\nabla^2 h_2 + w_1(h_1,h_2), \tag{47}$$

$$p_2 = -\sigma\nabla^2 h_2 + w_2(h_1,h_2), \tag{48}$$

$$w_1 = \frac{a_0 - a_1 - a_2}{h_2^3} + \frac{a_1}{h_1^3}, \tag{49}$$

$$w_2 = \frac{a_0 - a_1 - a_2}{h_2^3} + \frac{a_2}{(h_2 - h_1)^3}. \tag{50}$$

The non-dimensional expressions for the fluxes generated by the thermocapillary effect are:

$$\mathbf{q}_1^T = \frac{M}{2} h_1^2 \nabla[d(Bih_1 - \alpha\kappa)], \tag{51}$$

$$\mathbf{q}_2^T = \frac{M}{2}\{ -h_2^2\nabla(d\eta\alpha\kappa) + (2h_2 - h_1)h_1 \cdot \nabla\{d[Bih_1 - \alpha\kappa(1-\eta)]\}\}. \tag{52}$$

Here

$$M = \alpha_1(T_s - T_g)(H_1^0)^3\sqrt{\sigma_1^0}(6\pi/|A_{sg}|)^{3/2} \tag{53}$$

is the modified Marangoni number,

$$Bi = \frac{q\lambda_*}{\kappa_2} \tag{54}$$

is the Biot number (defined using the characteristic horizontal scale), and

$$d = [\kappa + Bi(1-\kappa)h_1 + Bi\kappa h_2]^{-1}, \tag{55}$$

$\eta = \eta_1/\eta_2$, $\sigma = \sigma_2^0/\sigma_1^0$, $a_0 = \mathrm{sign}(A_{sg})$, $a_1 = A_{s2}/|A_{sg}|$, $a_2 = A_{g1}/|A_{sg}|$.

We will use the problem (45) for studying the instabilities of plane ultra-thin films, $H_1 = H_1^0$, $H_2 = H_2^0$, and simulation of their nonlinear development.

3 Numerical simulations

3.1 Choice of parameters and numerical method

The system of equations (45) contains nine nondimensional parameters: M, Bi, σ, α, η, κ, a_0, a_1, and a_2. The Marangoni number is determined by the intensity of the external heating, the Biot number characterizes the heat transfer at the free boundary, while other six parameters are intrinsic characteristic of the multilayer system substrate/liquid 1/liquid 2/gas. Parameters α,η and σ are just ratios of physical parameters of the liquids, while a_0, a_1 and a_2 depend on the values of the Hamaker constants A_{sg}, A_{s2} and A_{g1}. The latter constants are determined by the dielectric permittivities of all the media as functions of the frequency (5), (4), and they depend mainly on the zero-frequency dielectric constants and high frequency refractive indices of the media (4), (11). It would be interesting to analyze the dependence of the dynamics of the system on all the relevant parameters. However, in the present paper we perform simulations only for the following set of parameters: $a_0 = 1$, $a_1 = -0.4$, $a_2 = -0.1$, $\eta = 1.2$, $\sigma = 0.8$, which corresponds to a *model* system formerly considered in (3).

This choice of parameters is caused by the following reasons. It is well known that in the case of a one-layer film, the van der Waals interaction typically leads to the film rupture. In order to avoid the film rupture, some regularizing modification of the disjoining potential is usually needed. In (3), it was found that for the set of parameters given above, the rupture is avoided even for pure van der Waals interactions. Instead of rupture, one observed a certain kind of “spinodal decomposition" of the film into localized droplets and a thin “precursor" film. This phenomenon has been established in (3) in the framework of the one-dimensional problem. The goal of the present paper is the investigation of this phenomenon in the presence of the Marangoni effect by means of full nonlinear simulations.

Evolution equations (45) have been discretized by central differences for spatial derivatives and solved using an explicit scheme. Periodic bound-

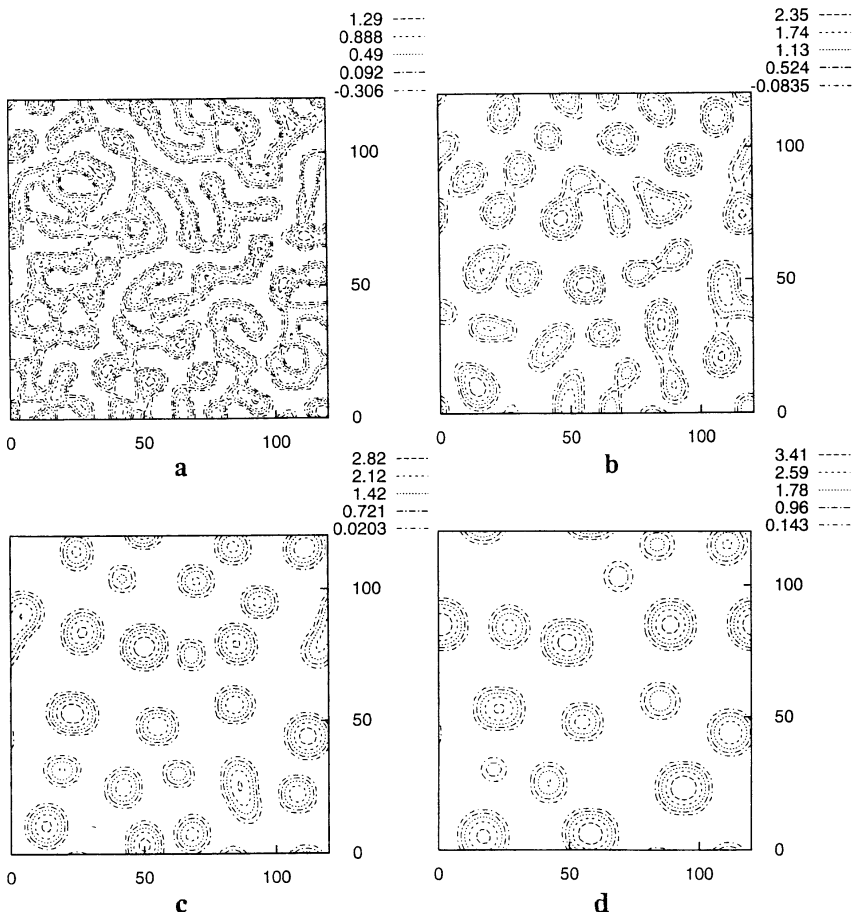

Figure 2: Isolines of $h_1(X,Y,T)-1$; (a) $T=330$; (b) $T=500$; (c) $T=800$; (d) $T=18000$; $M=0$; $h=1.2$.

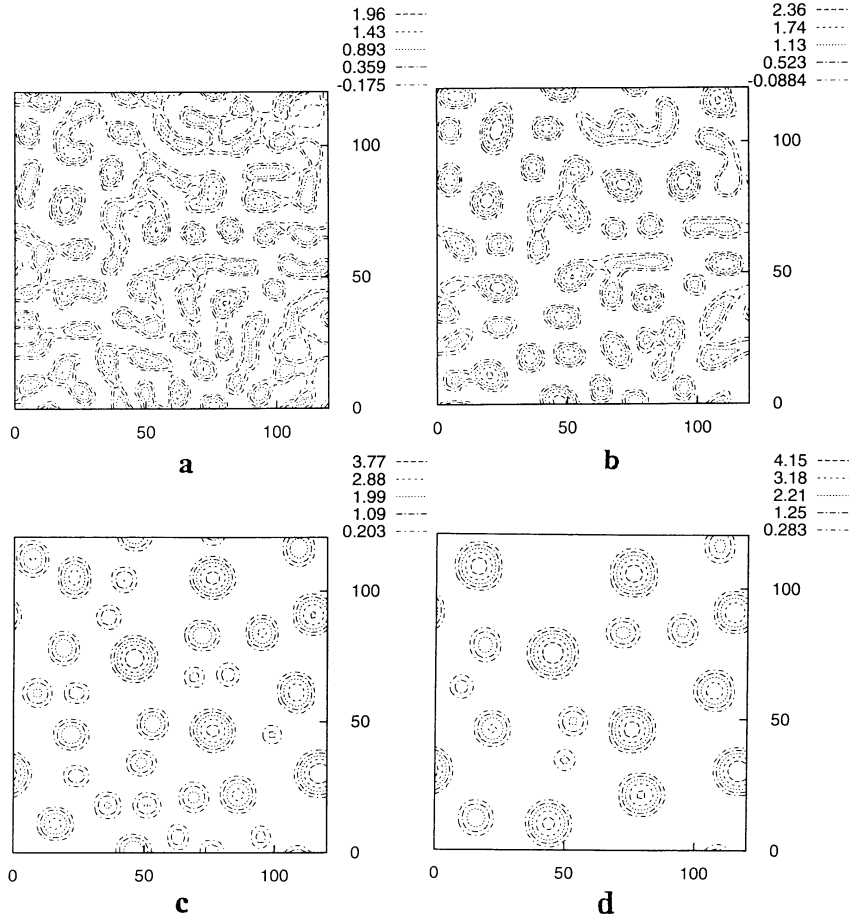

Figure 3: Isolines of $h_1(X,Y,T)-1$; (a) $T=240$; (b) $T=330$; (c) $T=800$; (d) $T=18000$; $M=1$; $h=1.2$.

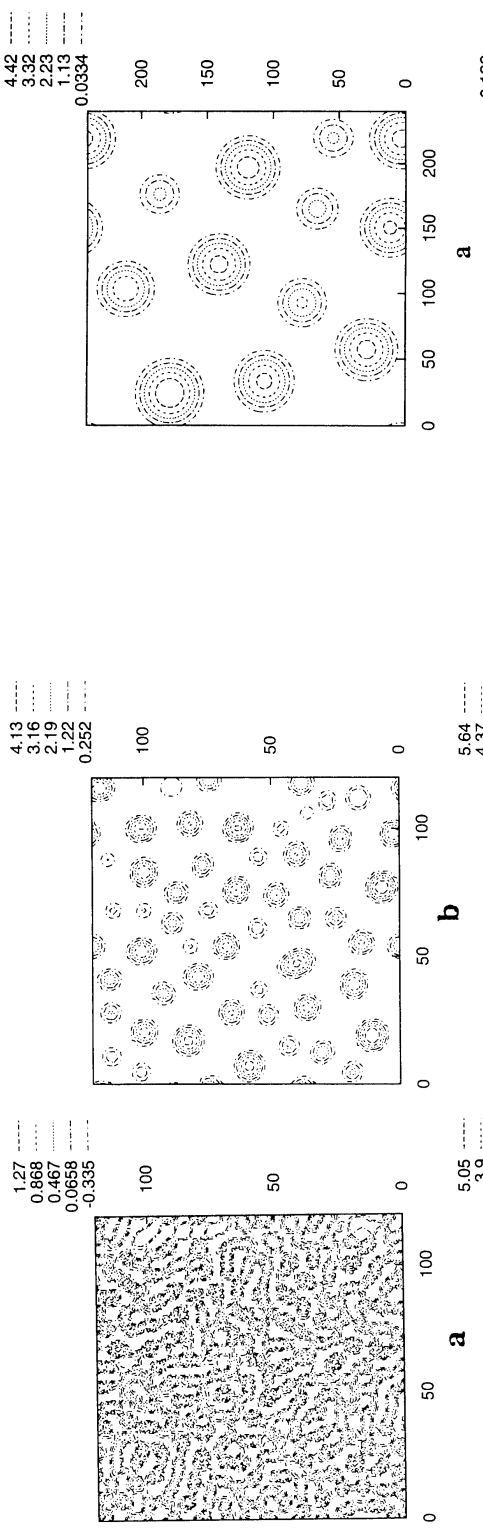

Figure 4: Isolines of $h_1(X,Y,T)-1$; (a) $T=60$; (b) $T=800$; (c) $T=18000$; (d) $T=30000$; $M=5$; $h=1.2$.

Figure 5: Isolines of $h_2(X,Y,T)-h$ (a) and $h_1(X,Y,T)-1$ (b); $T=22000$; $M=0$; $h=2.5$.

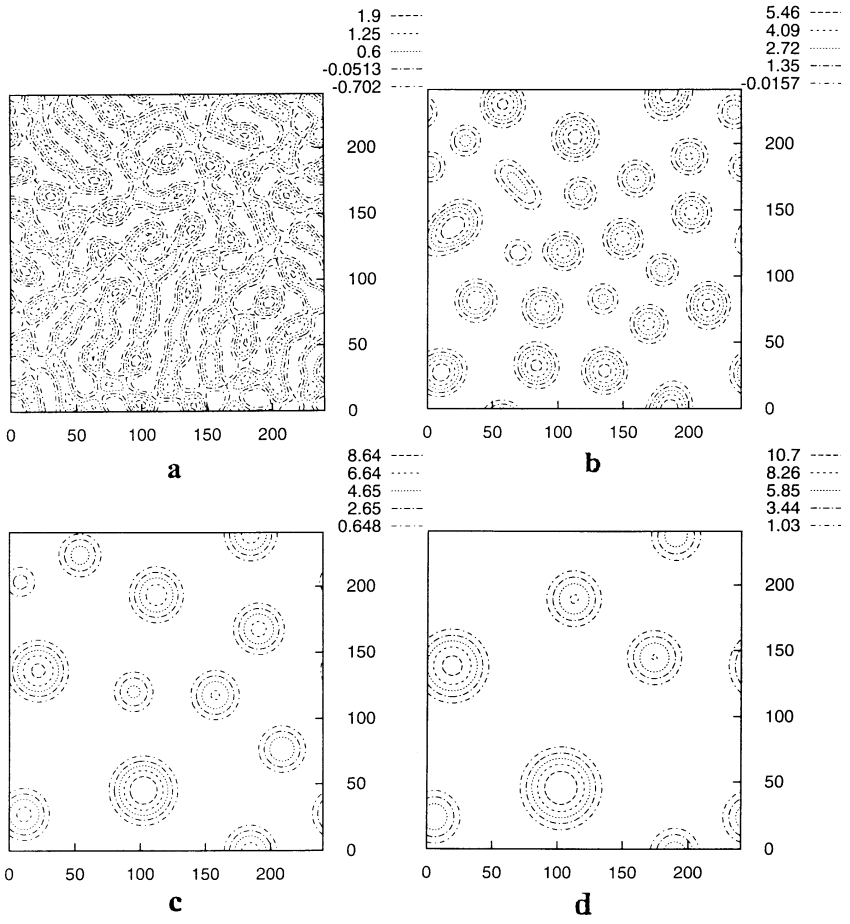

Figure 6: Isolines of $h_2(X,Y,T)-h$; (a) $T=800$; (b) $T=2800$; (c) $T=40000$; (d) $T=160000$; $M=1$; $h=2.5$.

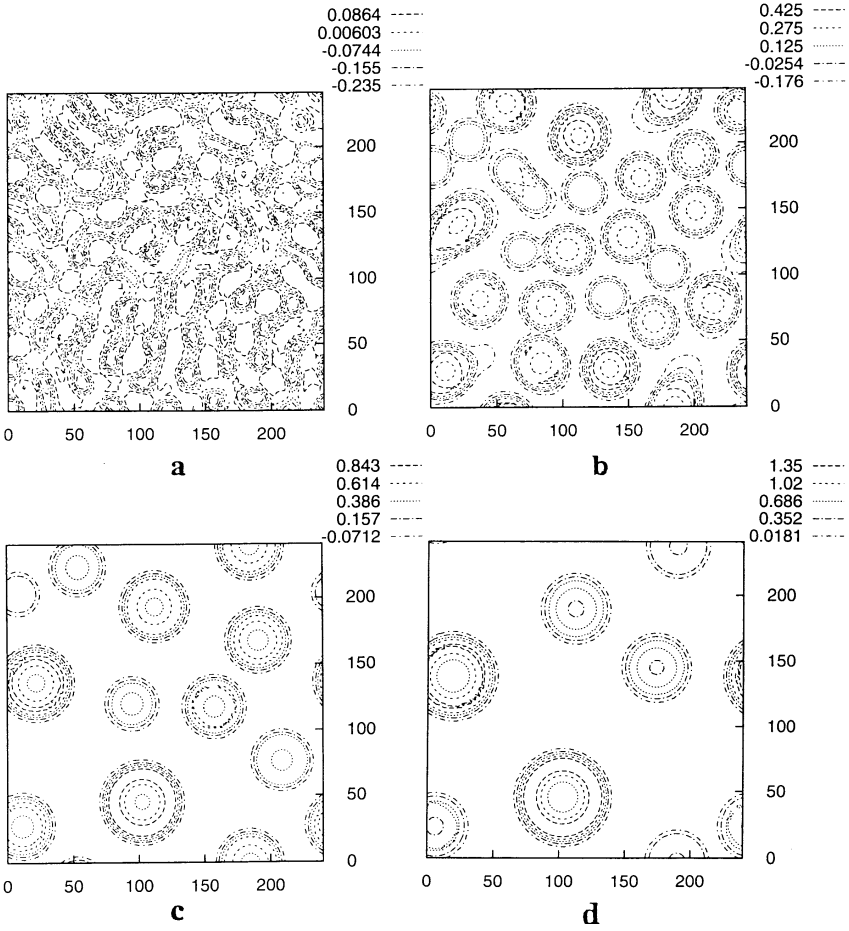

Figure 7: Isolines of $h_1(X,Y,T)-1$; (a) $T=800$; (b) $T=2800$; (c) $T=40000$; (d) $T=160000$; $M=1$; $h=2.5$.

ary conditions have been applied on the boundaries of the computational region. Initial conditions for h_j, $j = 1,2$ have been chosen in such a way that the mean value of $h_1(X,Y,0)$ was equal to 1 and the mean value of $h_2(X,Y,0)$ was equal to h, where $h > 1$. Hence, our computations depend on the additional geometric parameter, $h = H_2^0/H_1^0$. Small random deviations of $h_j(X,Y,0)$ from their mean values were imposed using a code creating pseudo-random numbers. We have chosen two different values of h: (i) $h = 1.2$; (ii) $h = 2.5$. The parameter $\alpha = 1$.

3.2 The case $h = 1.2$

The simulations have been carried out in the region 120×120 on the mesh 240×240.

First, let us remind the main stages of the films shape evolution observed in the absence of heating, $M = 0$ (see (7)). In the case $h = 1.2$, the shapes of both interfaces are quite similar. Therefore, it is sufficient to demonstrate only the evolution of the liquid-liquid interface, $h_1(X,Y,T)$. The main stages of the evolution are shown in Fig. 2. During a rather short period of time, the film is separated into two “phases", a “thick film" and a “thin film". The “thick" phase forms a percolating “labyrinthine" structure (Fig. 2(a)) with an approximately parabolic shape cross-section and a characteristic width of “rivulets" corresponding to the critical instability wavelength (see (3)). The “thin" phase consists of holes with flat bottoms. With the increase of time, the labyrinthine structure is destroyed into fragments and eventually separate droplets are formed (Figs. 2(b), 2(c), 2(d)). After the formation of droplets, a slow process of coarsening takes place. Two mechanisms of coarsening are observed. Some neighbor droplets coalesce (compare Fig. 2(c) with Fig. 2(d)). Also, small droplets dry out due to the Ostwald ripening.

Let us discuss now the influence of the Marangoni effect ($M > 0$, which corresponds to the case of heating from below for normal thermocapillary effect). The computations have been done for $Bi = 0.1$, $\kappa = 1$. The evolution of the system for $M = 1$ is shown in Fig. 3. The comparison of Fig. 2 and Fig. 3 reveals two effects. First, the development of the instability obviously becomes faster in the presence of heating (cf. Figs. 2(a) and 3(b)). Also, the characteristic spatial size of growing disturbances becomes smaller, and a number of small droplets is developed (cf. Figs. 2(c) and 3(c)). The hight of big droplets is larger in the presence of heating at the same instants of time.

The tendencies listed above become even more clear at larger values of the Marangoni number (see Fig. 4; $M = 5$). With the growth of M, the development of instabilities becomes faster, the area of droplets decreases, and their height grows.

3.3 The case $h = 2.5$

The simulations have been carried out in the region 240×240 on the mesh 400×400.

The typical shapes of droplets formed in the ab-

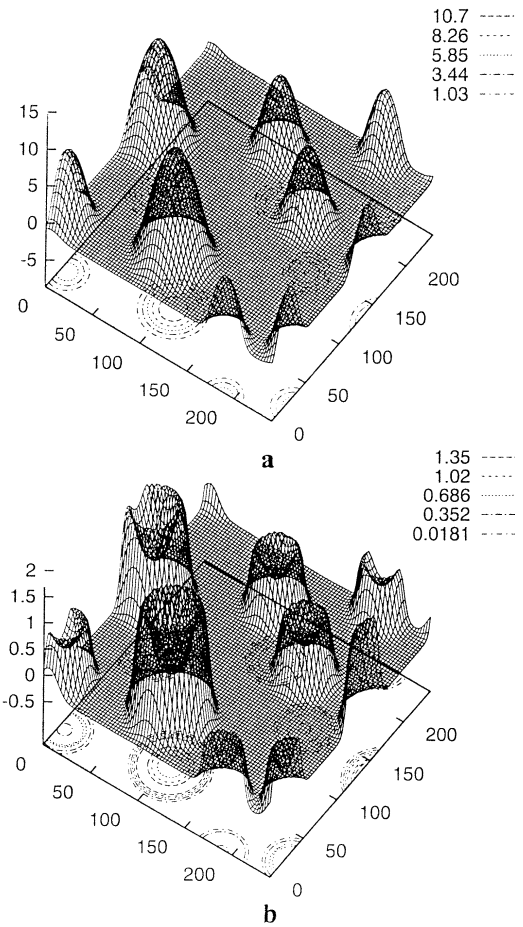

Figure 8: Shapes of the interfaces at $T = 160000$; (a) $h_2(X,Y,T)$; (b) $h_1(X,Y,T)$; $M = 1$; $h = 2.5$.

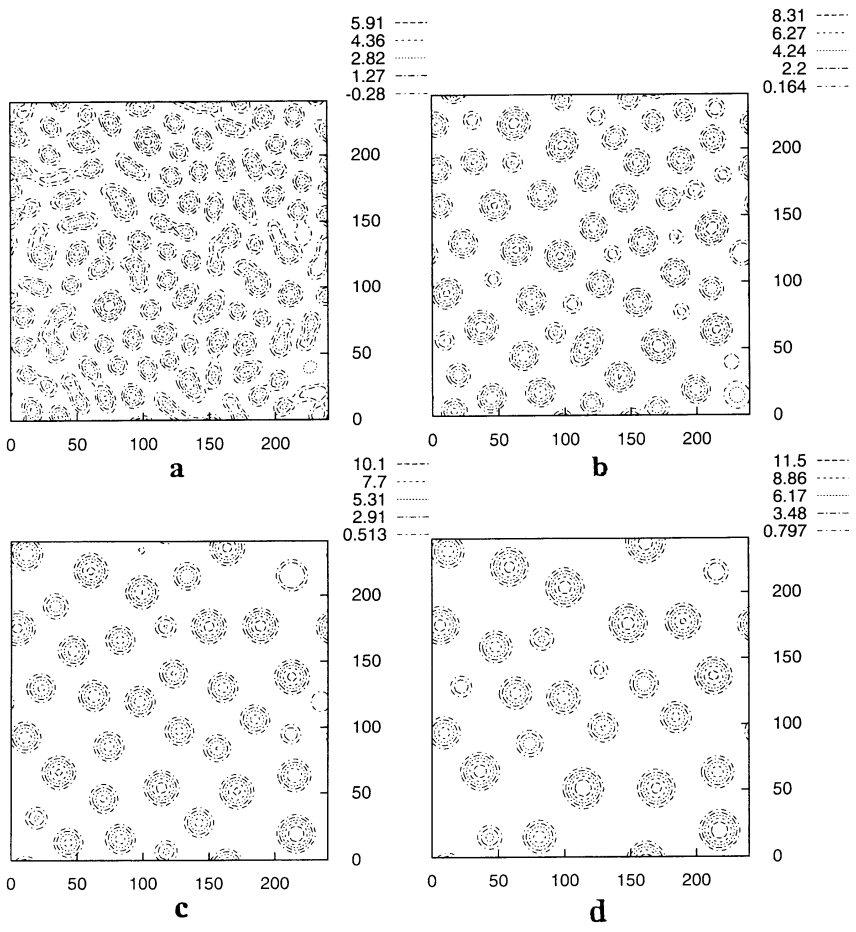

Figure 9: Isolines of $h_2(X,Y,T)-h$; (a) $T=210$; (b) $T=600$; (c) $T=5000$; (d) $T=40000$; $M=5$; $h=2.5$.

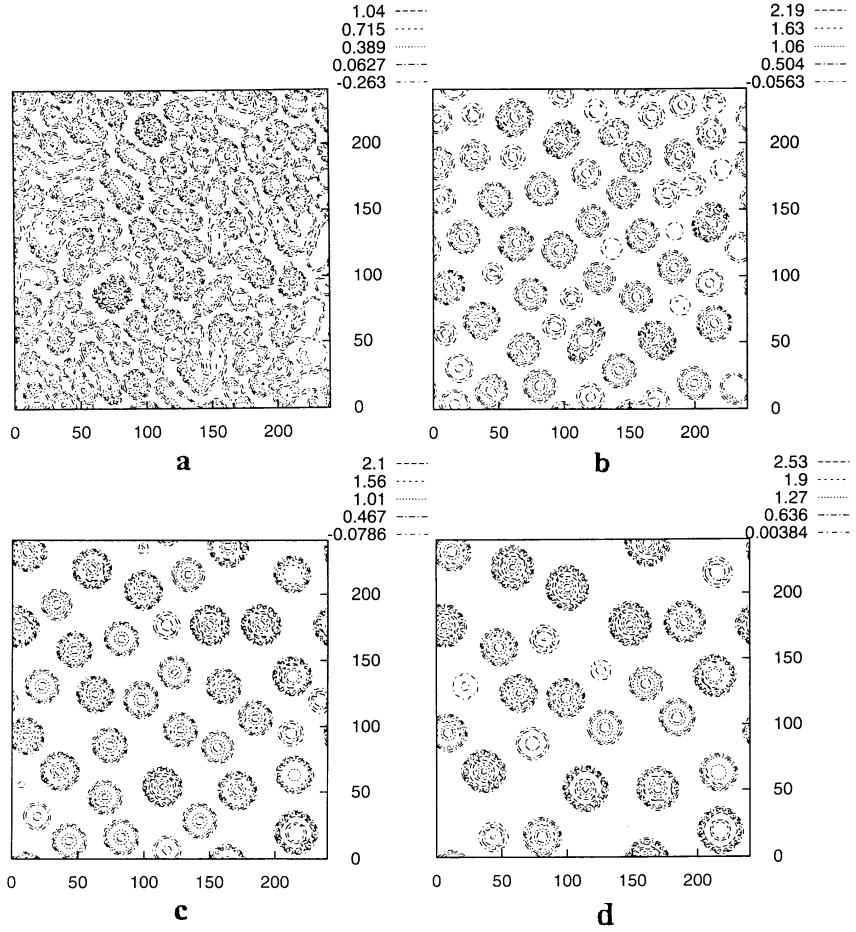

Figure 10: Isolines of $h_1(X,Y,T)-1$; (a) $T=210$; (b) $T=600$; (c) $T=5000$; (d) $T=40000$; $M=5$; $h=2.5$.

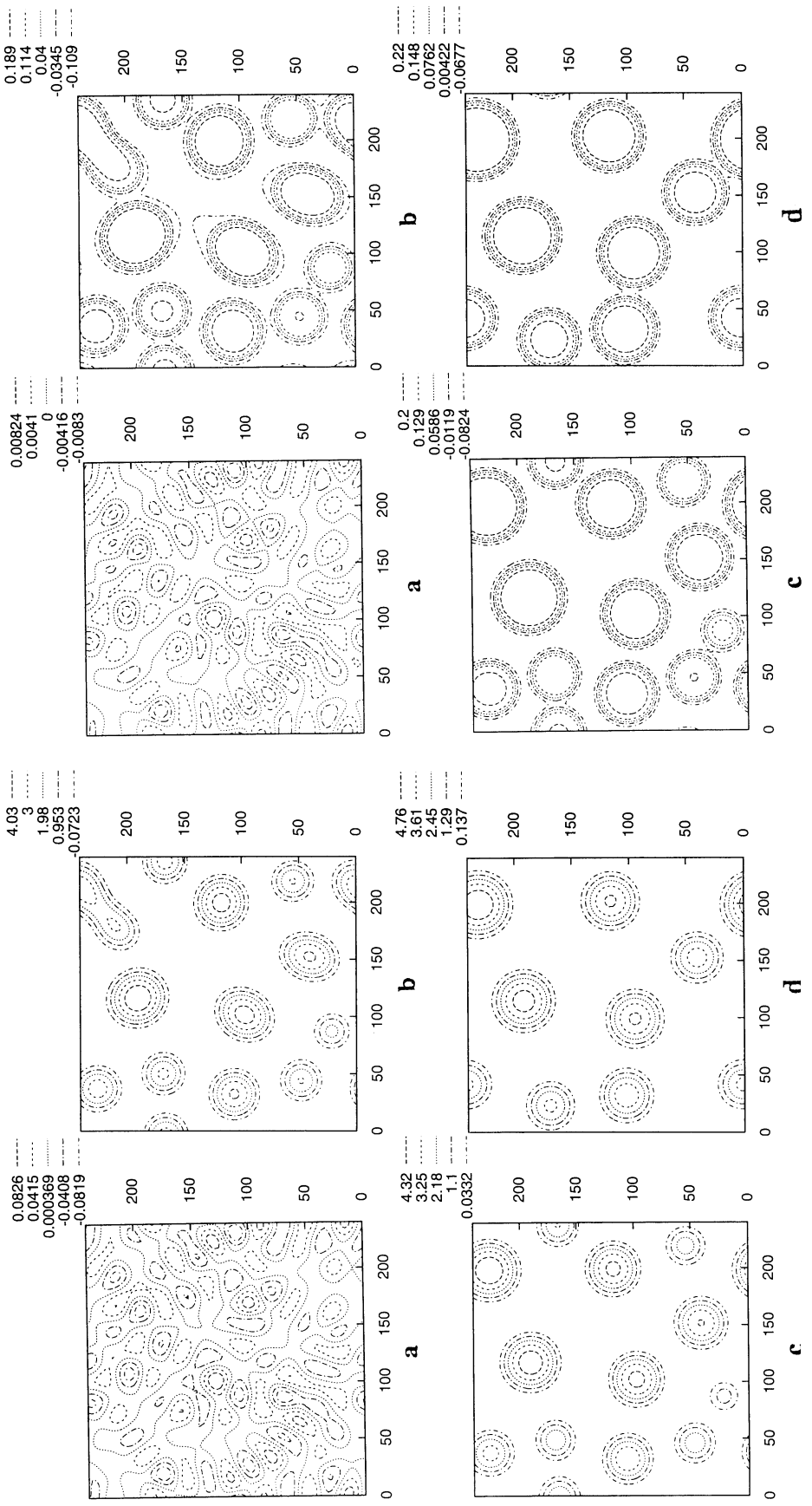

Figure 11: Isolines of $h_2(X,Y,T)-h$; (a) $T=1500$; (b) $T=10000$; (c) $T=20000$; (d) $T=80000$; $M=-0.1$; $h=2.5$.

Figure 12: Isolines of $h_1(X,Y,T)-1$; (a) $T=1500$; (b) $T=10000$; (c) $T=20000$; (d) $T=80000$; $M=-0.1$; $h=2.5$.

sence of heating ($M = 0$) are shown in Fig. 5. Let us emphasize that the deformation of the upper interface is much stronger than that of the lower interface, and the shapes of the interfaces are completely different. The deflection of the upper interface has a parabolic shape, while the deflection of the lower interface has a flat "plateau". The hight of the upper interface deformation is essentially larger than that of the lower interface. The structures are characterized by a larger characteristic length scale than in the case $h = 1.2$, and they develop slower.

In the case of heating ($M \neq 0$), the computations have been done for $Bi = 0.1$, $\kappa = 1$. The heating from below ($M > 0$) leads to the same qualitative changes of the instability development as in the case of $h = 1.2$: the instability is developed faster, the areas of droplets become smaller and their heights become larger (see Figs. 6 and 7; M=1). Let us emphasize that the shape of the liquid-liquid interface inside the droplet becomes non-monotonic (see Figs. 7 and 8(b)), so that this interface resembles an "inkpot". It is interesting to note that after the coalescence of droplets, the restoration of the axisymmetric shape of the structure is rather fast for the upper interface, while the axial asymmetry of the lower-interface structures takes much more time, and some crescent-like defects are clearly seen (see Fig. 7).

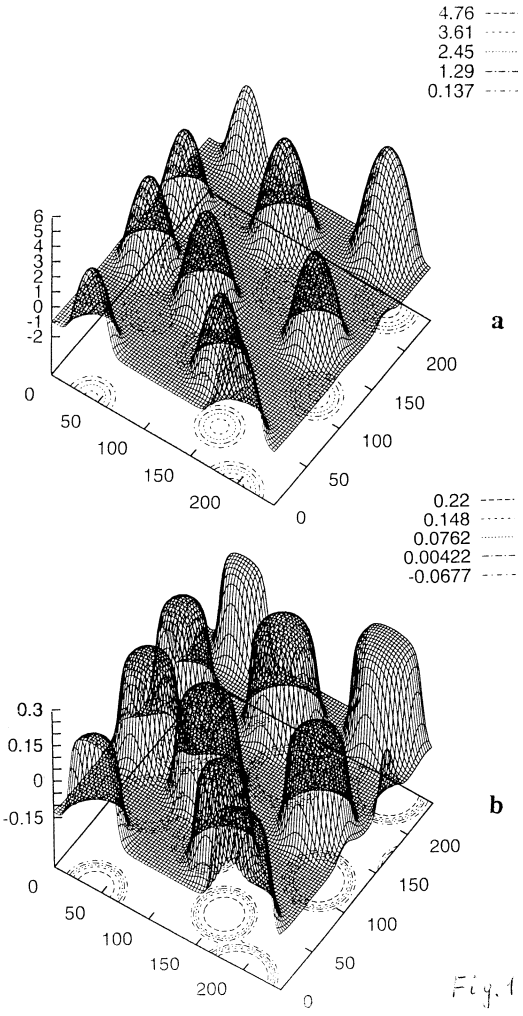

Figure 13: Shapes of the interfaces at $T = 8000$; (a) $h_2(X,Y,T)$; (b) $h_1(X,Y,T)$; $M = -0.1$; $h = 2.5$.

The growth of M leads to acceleration of the instability development and to the formation of small-scale structures (see Figs. 9 and 10). The distribution of sizes and heights of droplets is essentially polydisperse.

The heating from above ($M < 0$) leads to opposite changes in the process of the droplets development: the evolution becomes slower, and the characteristic size of structures increases. The evolution of interfaces at $M = -0.1$ is shown in Figs. 11 and 12. For larger values of $|M|$, $M < 0$, the instability is completely suppressed. The shape of the liquid-liquid interface becomes more round than in the absence of heating (see Fig. 13(b))

4 Conclusions

We have considered the decomposition of a two-layer film caused by intermolecular forces in the presence of the thermocapillary effect. We have found that heating from below leads to the acceleration of the decomposition, decrease of the characteristic lateral size of structures, and the increase of the droplets heights. Heating from above leads to slowing down the instability rate and eventually to a complete suppression of the instability. This observation shows that the instability threshold is achieved at a certain negative value of the Marangoni number, $M_c < 0$. The larger is the difference $M - M_c$, the higher is the characteristic growth rate of the instability. As it has been shown in (3), the instability generated by intermolecular forces takes place for

long waves with the wavenumbers in the interval $0 < k < k_m$. For longwave instabilities, the dependence $k_m \sim (M - M_c)^{1/2}$ is typical. This circumstance explains the decrease of the characteristic instability wavelength with the growth of M.

We have observed a nontrivial change of the droplet shape in the presence of the Marangoni effect, which manifests itself as the deformation of a "plateau" into an "inkpot".

References

Bandyopadhyay, D.; Gulabani, R.; Sharma, A. (2005): Instability and dynamics of thin liquid bilayers, *Ind. Eng. Chem. Res.* 44, 1259.

Davis, S. H. (1987): Thermocapillary instabilities, *Ann. Rev. Fluid Mech.* 19, 403.

Fisher L. S.; Golovin, A. A. (2005): Nonlinear stability analysis of a two-layer thin liquid film: Dewetting and autophobic behavior, *J. Coll. Interf. Sci.* 291, 515.

Israelachvili, J. N. (1992): *Intermolecular and Surface Forces*, Academic Press, New York.

Lifshitz, E. M.; Pitaevskii, L. P. (1980): *Statistical Physics*, Part 2, Pergamon, New York.

Merkt, D.; Pototsky, A.; Bestehorn, M.; Thiele, U. (2005): Long-wave theory of bounded two-layer films with a free liquid-liquid interface: Short- and long-time evolution, *Phys. Fluids* 17, 064104.

Nepomnyashchy, A. A.; Simanovskii, I. B. (2006): Decomposition of a two-layer thin liquid film flowing under the action of Marangoni stresses, *Phys. Fluids* 18, 112101.

Nepomnyashchy, A. A.; Simanovskii, I. B.; Legros, J. C. (2006): *Interfacial Convection in Multilayer Systems*, Springer, New York.

Oron, A.; Davis, S. H.; Bankoff, S. G. (1997): Long-scale evolution of thin liquid films, *Rev. Mod. Phys.* 69, 931.

Pototsky, A.; Bestehorn, M.; Merkt, D.; Thiele, U. (2004): Alternative pathways of dewetting for a thin liquid two-layer film, *Phys. Rev. E* 70, 025201.

Pototsky, A.; Bestehorn, M.; Merkt, D.; Thiele, U. (2005): Morphology changes in the evolution of liquid two-layer films, *J. Chem. Phys.* 122, 224711.

Pototsky, A.; Bestehorn, M.; Merkt, D.; Thiele, U. (2006): Evolution of interface patterns of three-dimensional two-layer liquid films, *Europhys. Lett.* 74, 665.

Simanovskii, I. B.; Nepomnyashchy, A. A. (1993): *Convective Instabilities in Systems with Interface*, Gordon and Breach, London.